Journal of Applied Polymer Science

Inherent porous structure modified by titanium dioxide nanoparticle incorporation and effect on the fouling behavior of hybrid poly(vinylidene fluoride) membranes

Hassan Younas,[1] Jiahui Shao,[1] Hongwei Bai,[2] Liyan Liu,[1] Yiliang He[1]
[1]School of Environmental Science and Engineering, Shanghai Jiao Tong University, Shanghai 200240, China
[2]Energy Research Institute, Nanyang Technological University, 637141, Singapore
Correspondence to: J. Shao (E-mail: jhshao@sjtu.edu.cn)

ABSTRACT: The incorporation of nanoparticles (NPs) into a casting solution is a widely used practice for controlling the membrane fouling tendency, but the specific role of NPs in fouling control from an internal porous structure optimization has seldom been investigated. In this study, we evaluated the specific role of titanium dioxide (TiO_2)–NPs (Degussa P25) in mitigating membrane organic fouling. We prepared the membranes by tailoring the concentrations of the NPs well; this resulted in an optimized membrane microstructure consisting of fingerlike voids (beneath the skin layer of the membrane) and spongy voids (adjacent to the fingerlike voids). The NP incorporation induced the formation of spongy voids beneath the skin layer, and the increase in the NP concentration increased the formation of spongy voids. Moreover, surface images obtained by scanning electron microscopy, X-ray photoelectron spectroscopy results, and contact angles confirmed that TiO_2–NPs were almost absent on the skin layer. Antifouling experiments were performed with a model organic foulant in two flow orientations [fingerlike voids facing the retentate (FVR) and spongy voids facing the retentate (SVR)]. The results show that the membrane fluxes in FVR decreased more than those in SVR. The membrane with 1.5 wt % TiO_2 operated in SVR exhibited the lowest flux decline; this suggested that spongy voids with TiO_2 exposure could mitigate fouling to a greater extent. © 2015 Wiley Periodicals, Inc. J. Appl. Polym. Sci. **2016**, *133*, 43265.

KEYWORDS: membranes; morphology; separation techniques

Received 22 September 2015; accepted 23 November 2015
DOI: 10.1002/app.43265

INTRODUCTION

Membrane filtration technology is one of the most noticeable water-treatment advances of recent years. However, membrane fouling is still a severe issue. Membrane modification via nanoparticle (NP) incorporation has proven to be an effective method for increasing the membrane fouling resistance.[1–5] Although the hydrophilicity of titanium dioxide (TiO_2)–NP blend membranes is not greatly increased and the contact angle remains almost unaffected, fouling mitigation has been observed to a great extent.[6–8] Song *et al.*[9] also reported an insignificant decrease in the contact angle (from 78 ± 0.8 to $74 \pm 0.5°$) and reduced deposition resistance of a poly(vinylidene fluoride) (PVDF)–poly(ethylene glycol) (PEG)–TiO_2 hybrid membrane. The presence of NPs in the membrane casting solution increased the viscosity of the dope solution, and the resulting membrane showed less fouling.[10] The decrease in the fouling of the NP blend membrane was attributed to the impact of the NPs. However, how these NPs significantly reduce the membrane fouling in polymer–NP hybrid membranes has rarely been investigated.

PVDF is a highly recommended organic polymer for the ultrafiltration (UF) process because of its excellent thermal stability and chemical resistance to radiation, organic solvents, acids, and bases. Although PVDF membranes usually have a good tensile strength and proper asymmetric structure for separation, it has hydrophobic characteristics. Various organic and inorganic materials, including PEG,[9,11,12] TiO_2–NPs,[9,13] silicon oxide–NPs,[14] and many others have been used to enhance the hydrophilicity of PVDF polymer membranes and, consequently, to reduce membrane fouling. TiO_2–NPs are preferred because of their distinct characteristics and their oxidation of a broad range of pollutants, including natural organic matters, phenolic compounds, pharmaceuticals, dye molecules, and microorganisms, with the potential production of CO_2 and H_2O as end products.[15–19] TiO_2 also improves the fouling resistance of membranes and induces a high rate of rejection of

Additional Supporting Information may be found in the online version of this article.

contaminants during filtration.[20,21] The incorporation of an optimized concentration of NPs is also considerable because a concentration of higher than 2% NPs increases the solution viscosity, hinders the complete degassing of the solution, and adversely affects the resulting membrane.[10] Despite that, it has also been reported that the polymer encases a large amount of NPs during physical blending, and a negligible amount of NPs is exposed to the surface.[14] The insignificant exposure of NPs to the membrane surface suggests that NPs probably play their role in the fouling resistance from the membrane matrix instead of the surface.

In addition to the hydrophilic modification of the membrane, the structure of the inherent porous network (voids) of the membrane also improves the fouling resistance. Several factors, such as the polymer type and concentration and the additive type and concentration, influence the voids underneath the membrane skin layer and, consequently, affect membrane fouling.[22] Bohonak and Zydney[23] observed that the existence of an intense microporous network structure at the solid–liquid interface increased membrane fouling resistance. Yeow *et al.*[22] described the existence of two kinds of porous structures (fingerlike voids and spongy voids) in PVDF membranes prepared with *N,N*-dimethylacetamide (DMAc) as a solvent, and the addition of an additive (PVP or PEG) favored the formation of fingerlike voids beneath the skin layer and increased the water flux. Oh *et al.*[24] found that a water–isopropyl alcohol mixture as a coagulant solvent favored the formation of spongy voids in PVDF membrane and decreased the fouling of the membrane. However, the potential impact of NPs on the porous structure of hybrid membranes has been studied less.

In this study, hybrid PVDF membranes were prepared with different concentrations of P25 TiO_2–NPs to increase the fouling resistance. We characterized the membranes to study their surface morphology, internal morphology, surface composition, elemental composition, and hydrophilicity with and without the inclusion of TiO_2–NPs. After we established that the addition of TiO_2–NPs supported the formation of spongy voids beneath the skin layer of the membrane, we performed UF experiments with two different flow orientations to assess the impact of the void structure on the antifouling performance of the membranes by examining the humic acid (HA) rejection, relative flux (RF), flux stability, flux recovery (FR), and fouling resistance. The two flow orientations in this study were the skin-side-up orientation and the skin-side-down orientation. HA was found to have a high fouling potential and, thus, has been used as a model compound for natural organic matter in many research studies. Therefore, HA was used in this study to examine the membrane fouling behavior.[25]

EXPERIMENTAL

Membrane Fabrication and Modification

The PVDF (SOLEF 6020, Solvay, Ltd.), PEG (molecular weight = 600 Da), TiO_2–NPs (P25, with an average size of 20–30 nm, Degussa Corp.), DMAc, ethanol, and HA (Aldrich Corp.) used in this study were analytical grade and were used as received.

Table I. Ratios of the Different Constituents of the Membrane Casting Solutions

	Constituent (wt %)			
Membrane	PVDF	PEG	TiO_2	DMAc
1	12	1	—	87
2	12	2	—	86
3	15	1	—	84
4	15	2	—	83
5	12	1	0.5	86.5
6	12	2	0.5	85.5
7	12	1	1.5	85.5
8	12	2	1.5	84.5
9	15	1	0.5	83.5
10	15	2	0.5	82.5
11	15	1	1.5	82.5
12	15	2	1.5	81.5

A set of two groups of membranes were prepared (there were 12 kinds of membranes in each group, M-1 to M-12) according to the constituent concentration given in Table I. The groups were designed on the basis of two flow orientations. In one flow orientation, filtration was done with the skin side up, that is, with the fingerlike voids (or macrovoids) facing the retentate (FVR). In the second flow orientation, filtration was done with the skin side down, that is, with spongy voids (or microvoids) facing the retentate (SVR). Correspondingly, membrane M-1 UF experiments with the skin side up and skin side down are referred as M-1–FVR and M-1–SVR, respectively. The phase-inversion process was used for membrane fabrication, as done by Song *et al.*,[11] where the membrane casting solution was prepared by the dissolution of a required quantity of PVDF, PEG, and TiO_2–NPs in DMAc. This was followed by overnight blending at 40°C and degassing at the same temperature overnight. The casting solution was cast on a glass plate at a casting knife height of 200 μm and a constant speed (1.2 m/min). The glass plate with the cast solution was immersed in pure water for gelation. The prepared membrane was transferred into pure water for a day to remove excessive solvent from the membrane.

Methods

HA (Aldrich Corp.) was dissolved in deionized water, and a 2 mg/L HA solution was used for the UF experiments. A laboratory-scale UF cross-flow system was designed and used to assess the membrane performance. A detailed schematic of the UF setup is given in Figure 1. The UF setup contained a 2-L reservoir for the feed solution (2 mg/L HA), and the feed solution was circulated in the membrane cell by a pump. The active membrane area for filtration was 48 cm^2 (8 × 6 cm^2), and the constant pressure (0.1 MPa) and flow rate (0.5 L/min) in the membrane cell was maintained by the regulation of the adjusters, as shown in the schematic in Figure 1. The photocatalytic activity was coupled with UF by the activation of the TiO_2–NPs under continuous exposure to UV light. A 100-W, high-pressure

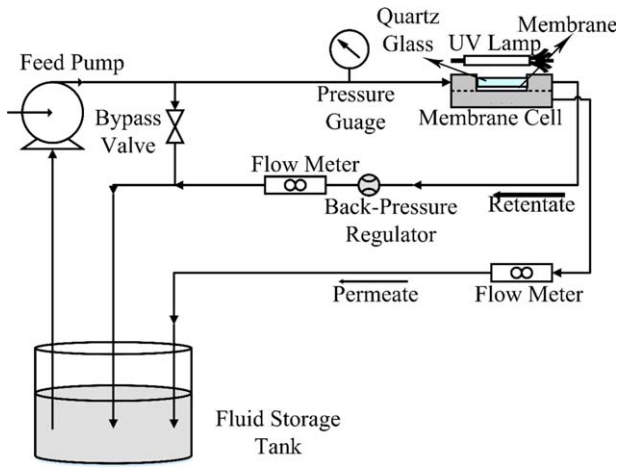

Figure 1. Schematic diagram of cross-flow UF coupled with a photocatalytic experiment. [Color figure can be viewed in the online issue, which is available at wileyonlinelibrary.com.]

mercury lamp (1.2 mW/cm^2) with a maximum light-emitting capacity of 365 nm (Bilon Corp., China) was used as the UV source.

Membrane Characterization

The surface morphology and internal structure of the prepared membranes were analyzed by scanning electron microscopy (SEM; FEI, Sirion 200) after pretreatment (Au sputtering) of cryogenically fractured dry membranes. The elemental composition of TiO_2 was determined with X-ray fluorescence (XRF) (Shimadzu, XRF-1800). The exposure of TiO_2 to the outer surface of the membranes was detected by X-ray photoelectron spectroscopy (XPS; Kratos, AXIS ULTRA DLD). The membrane hydrophilicity was indicated by the contact angle measurement with a goniometer (MAIST Vision, Dropmeter Professional A-200).

Evaluation of the Membrane Performance

The flux was determined according to eq. (1) as follows:

$$J = (1/A)(dV/dT) \tag{1}$$

where J is the permeate flux (L m^{-2} h^{-1}), A is the active membrane filtration area (m^2), V is the total volume of the permeate (m^3), and t is the filtration time (min).

The total resistance of the membrane (R_{Total}) during filtration was composed of different portions [eq. (2)]. A resistance-in-series model [eqs. (3–5)] was applied to quantify the relative influence of the intrinsic membrane resistance (R_m), irreversible fouling resistance (R_{if}), and resistance due to concentration polarization (R_{cp}):

$$R_{Total} = R_m + R_{if} + R_{cp} \tag{2}$$

$$R_m = \frac{\Delta P}{\mu J_w} \tag{3}$$

$$R_{if} = \frac{\Delta P}{\mu J_f} - R_m \tag{4}$$

$$R_{cp} = \frac{\Delta P}{\mu J_s} - R_m - R_{if} \tag{5}$$

where ΔP is the transmembrane pressure (0.1 MPa), μ is the pure water viscosity, J_w is the pure water flux of fresh membrane, J_f is the pure water flux of cleaned membrane, and J_s is the permeate flux during the filtration process.

The rejection coefficient for HA was calculated with the following equation:

$$R = \left(1 - \frac{C_p}{C_p}\right) \times 100\% \tag{6}$$

where C_p and C_f are the HA concentration in the permeate at a specified time during UF and the initial concentration of the feed, respectively. The HA concentration was evaluated with an ultraviolet–visible spectrophotometer (MAPADA Instruments Co., Ltd.) at 254 nm.[9,11]

RF of the membrane was calculated according to eq. (7). FR was calculated according to eq. (8)[26] after the physical cleaning (flushing with pure water) of the membrane:[14,27]

$$\text{RF}\,(\%) = \frac{J_s}{J_w} \times 100 \tag{7}$$

$$\text{FR}\,(\%) = \frac{J_f}{J_w} \times 100 \tag{8}$$

The flux decline occurring the during filtration experiment is termed the *overall flux decline* and can be measured as follows:

$$\text{Overall flux decline} = 100 - \text{RF} \tag{9}$$

Moreover, the irreversible flux decline and the reversible flux decline (caused by concentration polarization and/or a reversible adsorption phenomenon) can be calculated indirectly with eqs. (10) and (11), respectively:

$$\text{Irreversible flux decline} = 100 - \text{FR} \tag{10}$$

$$\text{Reversible flux decline} = \text{FR} - \text{RF} \tag{11}$$

RESULTS AND DISCUSSION

Impact of TiO_2 on the Microstructure of the Membrane

Cross-sectional SEM images with different concentrations of PVDF and TiO_2 (M-2, M-4, M-6, and M-8) are shown in Figure 2. It was clear that the membrane internal morphology had two types of porous networks: fingerlike voids (macrovoids) beneath skin layer of the membrane and spongy voids (microvoids) on the bottom side of the membrane; this varied with the concentrations of PVDF and TiO_2. Figure 2(a–d) presents cross-sectional SEM images for the membranes (without TiO_2) with different PVDF concentrations: 12% PVDF (M-2) and 15% PVDF (M-4). This indicated that a higher polymer concentration resulted in a compact porous network but insignificantly influenced the type of network. Yeow *et al.*[22] also reported that PVDF membranes prepared with DMAc produced macrovoids underneath the skin layer of the membranes, and the polymer concentration did not affect those macrovoids. However, the addition of TiO_2–NPs (0.5%) greatly decreased the macrovoids [Figure 2(e,f)], and a greater addition of TiO_2–NPs (1.5%) reduced more macrovoids, as shown in Figure 2(g,h). This indicated that the addition of TiO_2–NPs decreased and distorted the macrovoids in the membrane porous structure, and a higher concentration of TiO_2–NPs induced the existence of more microvoids in membrane inherent porous network. They reported that a high surface energy of SiO_2 NPs helped to bridge PVC polymer chains, and the resulting

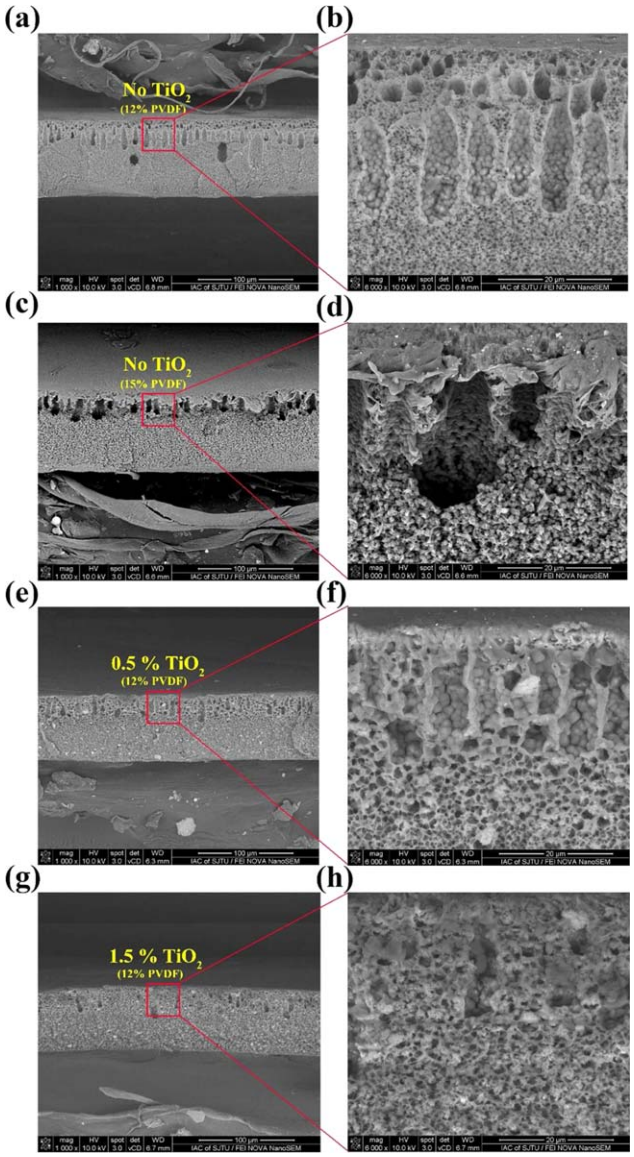

Figure 2. Cross-sectional SEM images of membranes with different concentrations of PVDF and TiO_2: (a,b) M-2 with 12% PVDF and without TiO_2, (c,d) M-4 with 15% PVDF and without TiO_2, (e,f) M-6 with 12% PVDF and 0.5% TiO_2, and (g,h) M-8 with 12% PVDF and 1.5% TiO_2. [Color figure can be viewed in the online issue, which is available at wileyonlinelibrary.com.]

membrane showed less fouling.[10] On the basis of that report, we assumed that the high surface energy of P25 TiO_2 (299 kJ/mol)[28] also helped to bridge the PVDF chains, and an increase in the NP concentration provided more bridging sites for PVDF. Moreover, many of the battery-based studies confirmed the possible interaction among the TiO_2–NPs and PVDF, where PVDF was applied as a binder for nano-TiO_2 or other ceramics.[29]

In addition to microstructural analysis, the elemental composition also assured that the membranes prepared with a high concentration of TiO_2 sustained a relatively higher amount of Ti. The elemental compositions of the membranes of 12% PVDF with different concentrations of TiO_2 (M-2, M-6, and M-8) were analyzed by XRF, and the data are provided in Table II.

Table II. Elemental Compositions of the Dry Membranes with 12% PVDF and Different Concentrations of TiO_2 (M-2, M-6, and M-8) by XRF Measurement

	Content (%)	
Membrane	F	TiO_2
M-2	99.62	0.0
M-6	85.48	14.16
M-8	72.92	26.70

The content (percentage) represented the relative concentration of TiO_2 to fluorine for the selective membrane. We found that the membrane with the higher TiO_2 concentration in the casting solution also contained a higher amount of TiO_2 inside the matrix. However, we noticed that the elemental composition data of the dry membranes presented in Table II were different from the concentration values in the casting solution; this was due to the solvent leaving the membrane matrix during the gelation of the casting solution.

Antifouling Prospects of the Membranes Corresponding to the Microstructure

Each of the 12 membranes (M-1 to M-12) was run first with pure water for 30 min to attain potential compaction and a constant pure water flux, and then, UF was done with the HA solution. The filtrate volume was collected at a regular interval of 10 min, and the flux was determined to correspond each filtrate sample. The normalized fluxes of the 12 membranes in the FVR flow orientations (with UV irradiation) are shown in Figure 3.

Figure 3 shows that membranes with higher PVDF concentrations showed fewer flux declines during the 90-min filtration process; this was in accordance with the reported results that the high PVDF content accounted for less flux decline because

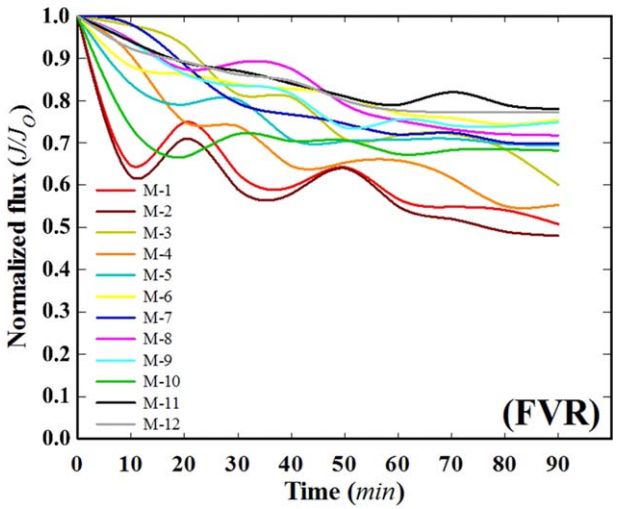

Figure 3. Normalized flux of 12 membranes during the UF of FVR flow orientation with UV irradiation. J = flux at any time; Jo = flux at the start of the experiment. [Color figure can be viewed in the online issue, which is available at wileyonlinelibrary.com.]

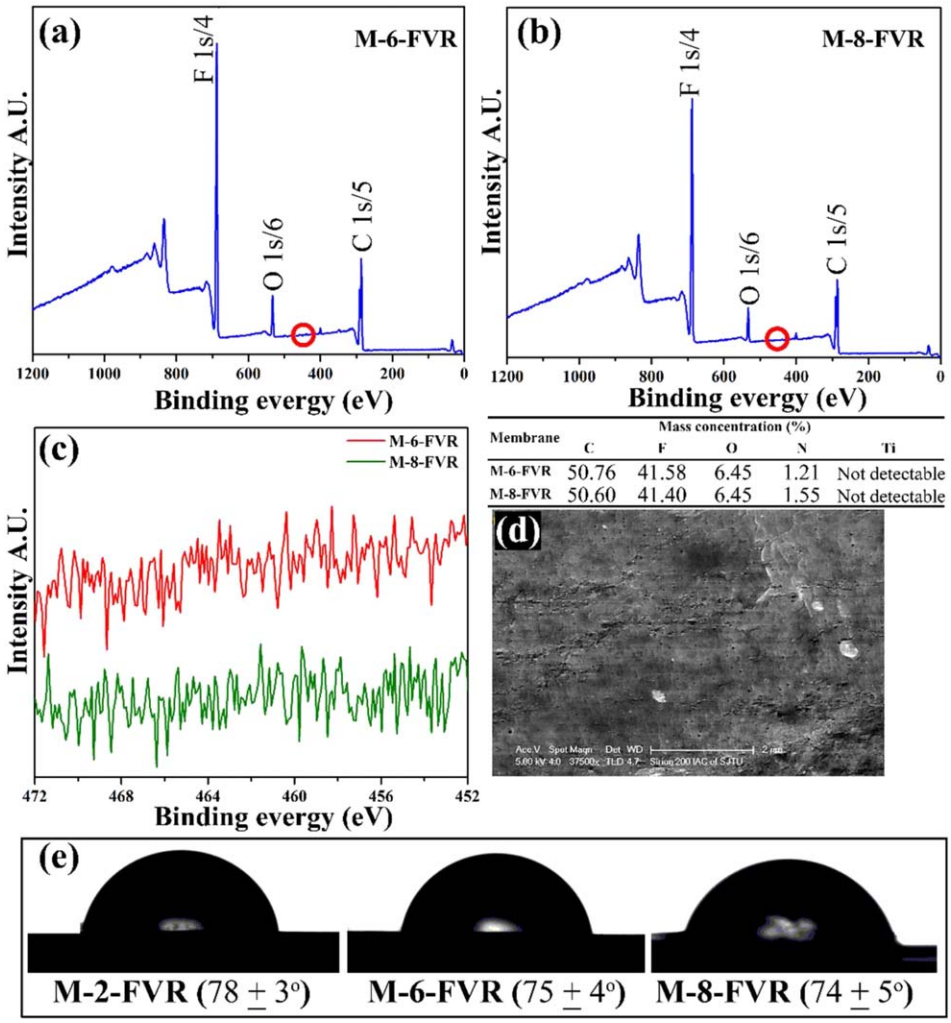

Membrane	Mass concentration (%) C	F	O	N	Ti
M-6-FVR	50.76	41.58	6.45	1.21	Not detectable
M-8-FVR	50.60	41.40	6.45	1.55	Not detectable

Figure 4. Surface analysis of the presence of TiO_2 on the skin-side-up surface. (a,b) XPS spectrum of all the components of the membranes (M-6–FVR and M-8–FVR, respectively). (c) The binding energy region in which Ti gave the peak was separated and analyzed further for any presence of Ti. (d) SEM surface image of M-8–FVR. The quantitative measurements of the components are also given in the table. (e) Contact angle measurements of the membranes based on the TiO_2 concentration. [Color figure can be viewed in the online issue, which is available at wileyonlinelibrary.com.]

of the smaller pore size.[30] Figure 3 also shows that all of the TiO_2 containing membranes (M-5–FVR to M-12–FVR) had less flux decline than the PVDF membranes without TiO_2–NPs (M-1–FVR to M-4–FVR); this could have been due to the hydrophilic impact of TiO_2, UV activation of TiO_2 on the surface of the membrane, or the membrane structural transformation (Figure 2) with the addition of TiO_2.

The observed fluctuation in the normalized flux values (Figure 3) was speculated by the following reactions[31]:

$$DOM + h\nu \rightarrow {}^3DOM^* \rightarrow {}^3DOM^* + O_2 \rightarrow DOM^* + 0_2^{\circ -} \quad (12)$$

$$0_2^{\circ -} + H^+ \rightarrow H0_2^{\circ -} \rightarrow 0_2^{\circ -} + H0_2^{\circ} + H_2O \xrightarrow{h\nu} H_2O_2 \xrightarrow{h\nu} OH^{\circ} + OH^{\circ} \quad (13)$$

The dissolved organic matter (DOM)—HA was DOM in this case[31]. It was converted into triplet state under light ($^3DOM^*$); this oxidized the oxygen molecule into a superoxide radical anion ($O_2^{\circ -}$). $O_2^{\circ -}$ produced the perhydroxy radical (HO_2°) and finally hydroxyl radicals (OH°). The presence of OH° increased the water uptake,[32] and OH° together with $O_2^{\circ -}$ oxidized the organic pollutant.[33] We considered that HA (accumulated in the membrane pores) produced OH°; this attracted more water molecules and caused fluctuations in the flux.

To analyze the aforementioned considerations about the smaller flux decline for TiO_2-containing membranes, the membrane surfaces were characterized for the detection of TiO_2. The selected membranes contained 12% PVDF and different concentrations of TiO_2 [M-6–FVR (0.5%) and M-8–FVR (1.5%)]. The XPS analysis revealed that none of the M-6 and M-8 membranes gave any indication of Ti presence on the surface with skin side up or FVR flow orientation, neither qualitatively [Figure 4(a–c)] nor quantitatively (see the table in Figure 4). We also observed, as shown in Figure 4(d), that the SEM surface image of the membrane with 1.5% TiO_2 barely showed the presence of any TiO_2. These findings supported the fact that the polymer encased a huge number of NPs, and only a small number of NPs were exposed on the surface of the membrane. This failed to express the true impact of the NPs.[14,34] Figure 4

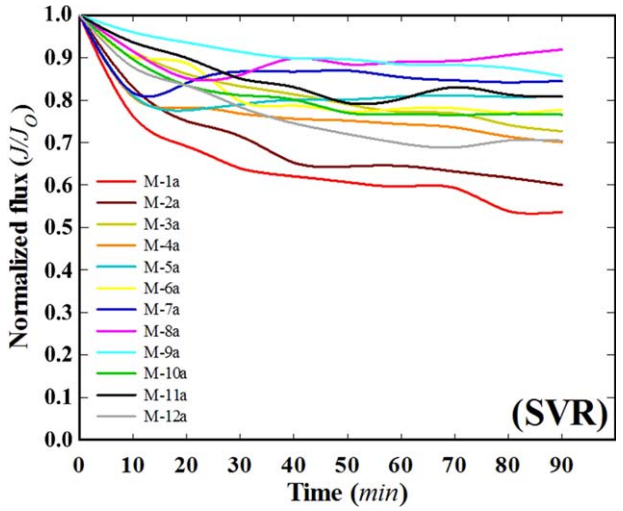

Figure 5. Normalized flux of 12 membranes during the UF of SVR flow orientation with UV irradiation. J = flux at any time; Jo = flux at the start of the experiment. [Color figure can be viewed in the online issue, which is available at wileyonlinelibrary.com.]

indicates that the TiO_2–NPs were almost absent on the top surface of the membrane (FVR flow orientation). In addition, no noticeable change in the contact angle was observed with different concentrations of TiO_2 [Figure 4(e)]; this was in agreement with the previous findings.[6] At the same time, the addition of the TiO_2–NPs transformed the macrovoids into microvoids beneath skin layer of the membrane and reduced the flux decline. Therefore, structural transformation was responsible for the smaller flux decline; the structure was transformed from macrovoids to microvoids because of the addition of TiO_2 and the concentration of TiO_2. The lowest flux decline of 20% was observed on the M-11–FVR membrane, where all of the constituents of the membrane (high PVDF, low PEG, and high TiO_2–NP concentration) supported the existence of more microvoids as an inherent porous network of the membrane.

The results in Figure 3 indicates that the membrane exhibited a smaller flux decline with more microvoids beneath the skin layer. To support the behavior of the microvoids toward a smaller flux decline, UF experiments were conducted in the SVR flow orientation because SVR with microvoids of the membrane facing the retentate solution. Indeed, a smaller flux decline was observed for each of the 12 membranes (Figure 5) with the SVR flow orientation as compared to the membrane with the FVR flow orientation (Figure 3). Bohonak and Zydney[23] also observed that a smaller flux decline occurred during skin-side-down flow orientation because the foulant particles were more likely to be deposited on the external membrane surface, and the rich interconnected porous substructure of the membrane prevented the access of small particles (in the feed solution) to the pores of the skin layer to reduce fouling. In this study, we found that TiO_2-containing skin-side-down membranes or the SVR flow orientation accounted for even less flux decline than membranes without TiO_2. The possible reason is explained in Figure 6. The lowest flux decline (10%) was recorded for a low PVDF concentration (12%) and high TiO_2–NP concentration (1.5%).

Figure 6 shows the results obtained for the detection of TiO_2 on the surface of the membranes with 12% PVDF and different concentrations of TiO_2 [M-6–SVR (0.5%) and M-8–SVR (1.5%)] during SVR flow orientation. The TiO_2 was detected on the bottom surface of the membranes. Although in the XPS full spectrum [Figure 6(a,b)], neither of the membranes produced any qualitative peaks of Ti, a sharp increase occurred in the intensity of O1s/6 for M-8–SVR [Figure 6(b)]. The increase in the O1s/6 intensity was attributed to TiO_2 as an additional source of O1s/6. This was consistent with the fact that the Ti peak was clearly distinguished in deconvolution only in M-8–SVR [Figure 6(c)], where the Ti binding energy region was separated and focused. In terms of quantification, XPS data analysis (shown in the table in Figure 6) showed that M-6–SVR contained a negligible amount of Ti (0.07%) on the outer surface, whereas M-8–SVR contained 0.25% Ti. The SEM surface image of M-8–SVR [Figure 6(d)] also confirmed the presence of TiO_2 on the bottom surface of the membrane; the SEM results were consistent with the XPS finding that more TiO_2–NPs were exposed on the bottom surface of the membrane. The concentration of TiO_2 detected on the bottom surface was proportional to the concentration added in the casting solution (when more TiO_2 was added, more TiO_2 appeared at the bottom). This was verified by the XPS results and contact angle measurements. When the concentration of TiO_2 was 0.5%, the contact angle was measured to be 64 ($\pm 4°$), and the contact angle was reduced to 57 ($\pm 4°$) when the TiO_2 concentration was increased to 1.5% [Figure 6(e)]. The decrease in the contact angle accounted for the higher hydrophilicity. The uneven distribution and the nonuniform exposure of TiO_2 to the membrane matrix and membrane surface were also observed elsewhere in SEM images.[9,11,34]

Hence, we confirmed that the decrease in the flux decline (for TiO_2-containing membranes during the SVR flow orientation) was the combined effect of spongy voids as the solid–liquid interface and the impact of TiO_2 itself, which was absent in the FVR flow orientation. This was further verified by a comparison of the flux declines of the M-2–SVR and M-8–SVR membranes (Figure 5). Both membranes were prepared from analogous casting solutions except for the addition of 1.5% TiO_2–NPs in M-8–SVR, and a smaller flux decline was observed with the M-8–SVR membrane.

HA Rejection in the Two Flow Orientations

Figure 7 shows the rejection of 2 mg/L HA at the end of the 90-min UF experiment with UV irradiation in the FVR and SVR flow orientations. HA rejection was determined at a regular interval of 10 min, and the detailed rejection data of HA as a factor of the time are given in the Supporting Information (Figure S1). After a complete cycle of UF (90 min), 80–90% of HA rejection was achieved with both flow orientations. The rejection of HA increased as a factor of the time and reached a steady state (ca. 80%) with the neat PVDF membranes, whereas the HA rejection was relatively higher from the beginning of the UF experiment with TiO_2-containing membranes. Devi *et al.*[35] also observed a higher pollutant rejection with TiO_2–NP-containing membranes. They explained that the TiO_2–NPs shortened interconnected passages in the membrane matrix because

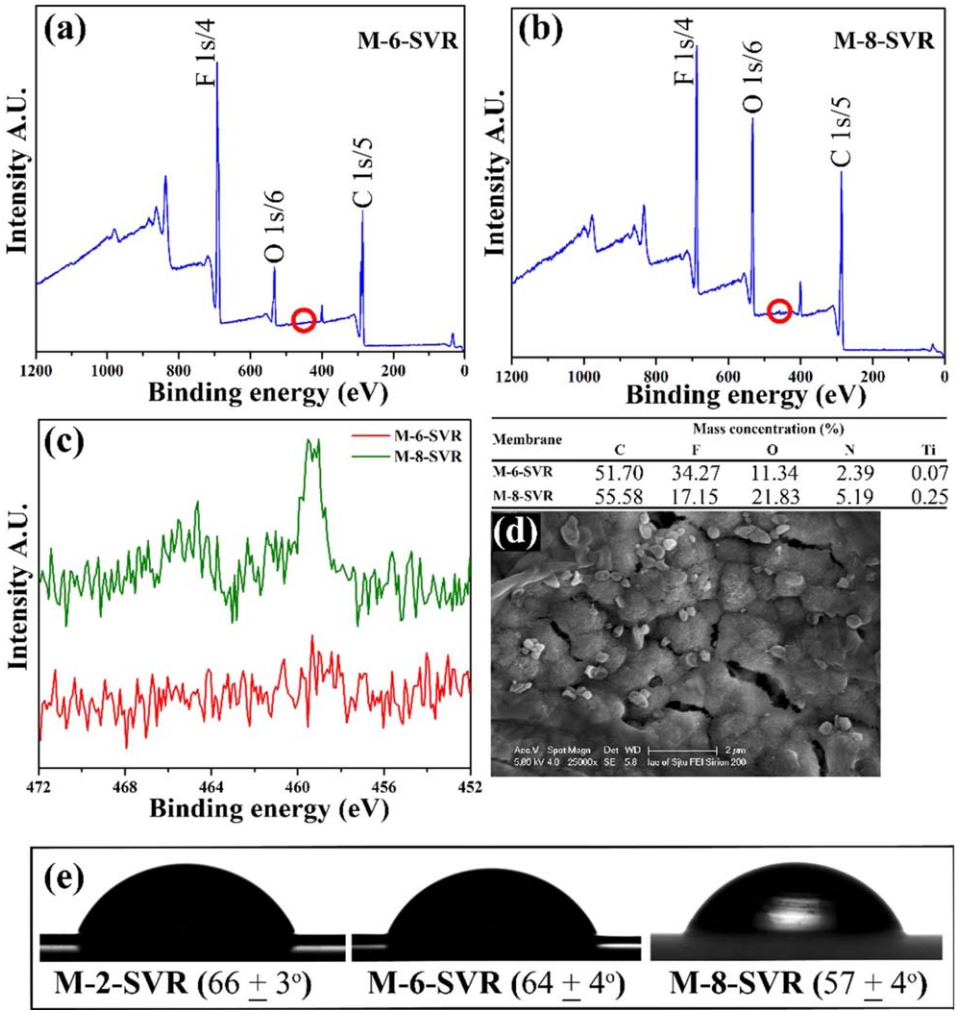

Figure 6. Surface analysis of the presence of TiO_2 on the skin-side-down surface. (a,b) XPS spectrum of all of the components of the membranes (M-6–SVR and M-8–SVR, respectively). (c) The binding energy region in which Ti gave the peak was separated and further analyzed for any presence of Ti. (d) SEM surface image of M-8–SVR. The quantitative measurements of the components are also given in the table. (e) Contact angle measurements of membranes on the basis of the TiO_2 concentration. [Color figure can be viewed in the online issue, which is available at wileyonlinelibrary.com.]

of successive agglomeration, and this resulted in a higher pollutant rejection.

As shown in Figure 7, membranes M-1–SVR to M-4–SVR (without TiO_2–NPs) showed the lowest HA rejection; the maximum HA rejections (90%) were observed in membranes M-5–SVR to M-12–SVR (the TiO_2-containing membranes). As observed in the SEM images and XPS analysis, the TiO_2–NPs were more inclined to be concentrated on the bottom surface of the membrane, and the SVR flow orientation allowed the TiO_2–NPs to be in direct contact with the HA molecules. These HA molecules could be considerably adsorbed onto the TiO_2–NPs.[36] As a result of the absorbance of HA on TiO_2, two phenomenon occurred. The pores may have narrowed; which prevented further HA molecules from accessing the membrane matrix and finally increased the HA rejection.[37] Alternatively, the adsorbed HA produced foulant–foulant electrostatic repulsion, which caused concentration polarization at the surface and increased HA rejection. In the former case, less FR should have occurred

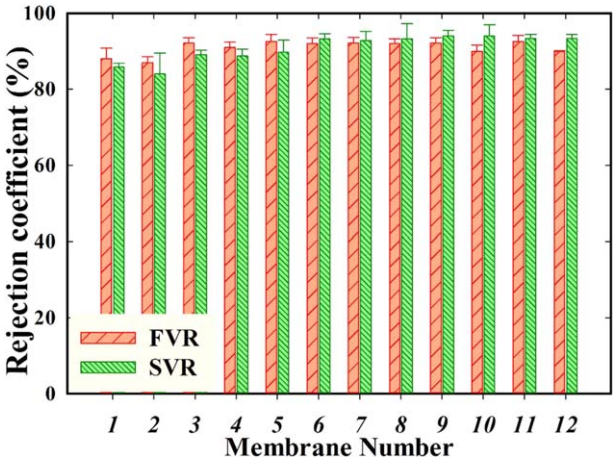

Figure 7. Rejection of 2 mg/L HA in a UF experiment with UV irradiation in two flow orientations. [Color figure can be viewed in the online issue, which is available at wileyonlinelibrary.com.]

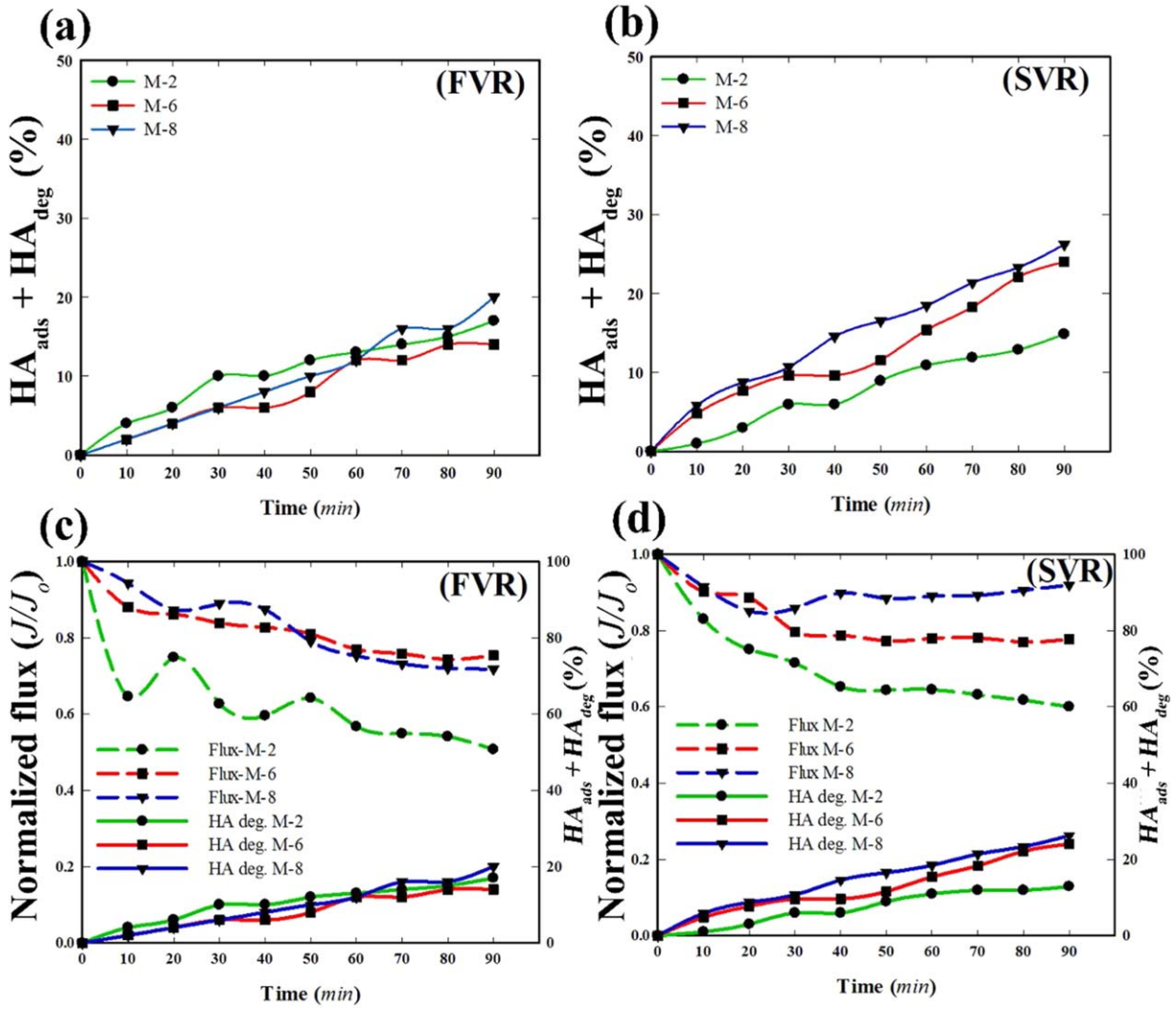

Figure 8. Reduction of HA in a feed solution and normalized flux during a photocatalytic UF process in the FVR and SVR flow orientations. HA_{ads} and HA_{deg} = adsorption of HA and degradation of HA, respectively. [Color figure can be viewed in the online issue, which is available at wileyonlinelibrary.com.]

($R_{if} > R_{cp}$). In the latter case, a high FR should have occurred ($R_{if} < R_{cp}$). This is explained in detail in the last section (Figure 12, shown later). Overall, we found that the HA rejection was not compromised in the SVR flow orientation.

TiO_2 as a Photocatalyst for HA Degradation

We illustrated the photocatalytic activity of the TiO_2–NPs in the membranes by monitoring the amount of HA in the feed solution during the UF experiment. The complete data of the photocatalytic degradation of HA molecules by all of the membranes are shown in the Supporting Information (Figure S2). Figure 8 shows the photocatalysis results for the 12% PVDF membranes with TiO_2 concentrations of 0, 0.5, and 1.5%. Figure 8(a) shows an HA reduction of about 20% in the feed with the FVR flow orientation at the end of the UF experiment. Membrane M-2–FVR did not contain TiO_2–NPs; therefore, the HA concentration was reduced only because of the adsorption of HA molecules, and a decrease in the flux occurred [Figure 8(c)] because of the deposition of HA on the surface of the membrane and/or inside the membrane pores. At the same time, the presence of TiO_2–NPs in membranes M-6–FVR and M-8–FVR degraded the HA molecules; therefore, the HA reduction was caused by both the degradation and adsorption of HA molecules. An almost similar amount of HA was reduced from the feed tank in the case of M-2–FVR, M-6–FVR, and M-8–FVR, but a smaller flux decline occurred for M-6–FVR and M-8–FVR than for M-2–FVR. This could have been due to the photocatalytic degradation of HA molecules. Song and coworkers[9,11] also reported the photocatalytic degradation of HA on the membrane surface, although they studied it for the self-cleaning capability of the fouled membranes. Figure 8(b) shows that the 12% HA concentration was reduced during filtration with the M-2–SVR membrane (without TiO_2), whereas the 25% HA concentration was reduced during filtration with M-6–SVR (with 0.5% TiO_2) and M-8–SVR (1.5% TiO_2). A higher HA reduction was observed for membranes with TiO_2 in the SVR flow orientation than for membranes with TiO_2 in the FVR flow orientation; this was consistent with the fact that TiO_2–NPs were more inclined to be concentrated on the bottom surface. Hence, more photocatalytic degradation of HA occurred

Figure 9. Surface changes of the membranes after 90 min of photocatalytic UF: (a) M-2–FVR, (b) M-8–FVR, and (c) M-8–SVR. [Color figure can be viewed in the online issue, which is available at wileyonlinelibrary.com.]

with SVR. Also, the higher amount of TiO_2 in the membrane accounted for the smaller flux decline, as shown in Figure 8(d). At the end of 90 min of UF, the flux decline was recorded in the following order: M-2–SVR > M-6–SVR > M-8–SVR. This indicated that more TiO_2–NPs were exposed to the outer surface, more reactive oxygen species were produced, more HA was degraded, and less fouling occurred. Any of the reactive oxygen species (OH°, $O_2^{\circ -}$) could oxidize HA that was produced during the photoactivation of TiO_2. The post-UF surface analysis of the membranes is also shown in Figure 9, and the adsorption and degradation of HA could be differentiated from the colors of the different membranes.

Photoinduced Hydrophilicity of the Membranes with TiO_2–NPs

Figure 10 shows the actual fluxes of membranes (M-2, M-6, and M-8) with different TiO_2 concentrations of 0, 0.5, and 1.5%, respectively, after 90 min of filtration of 2 mg/L HA with UV irradiation. The filtrate flux values of all 12 membranes after the 90-min UF experiment are given in the Supporting Information (Figure S3). We observed that for both the FVR and SVR flow orientations, the actual fluxes of the TiO_2-containing membranes (M-6 and M-8) were higher than that of membrane without TiO_2 (M-2). This could be explained by the fact that the TiO_2-containing membranes possessed both a water-uptake capability and photocatalytic degradation capability for HA because of its blended TiO_2 in the membrane matrix.[32,38]

Both membranes (M-6–FVR and M-8–FVR) had similar fluxes of about 100 L m^{-2} h^{-1} bar^{-1}, although they contained different concentration of NPs. This suggests that the concentration of TiO_2 played a nondeterministic role in the flux increase in the case of the FVR flow orientation. On contrary, in the SVR flow orientation, the membrane with the high TiO_2 concentration (M-8–SVR) produced a higher flux, and the membrane with the low TiO_2 concentration (M-6–SVR) produced a lower flux. Because the previous XPS and SEM analyses showed that the TiO_2–NPs were barely observed on the top surface of the membrane (the FVR flow orientation) and the TiO_2–NPs were more inclined to be concentrated on the bottom surface of the membrane (the SVR flow orientation), we concluded that the effect of the TiO_2 concentration on the flux enhancement was lower for the FVR flow orientation than for the SVR flow orientation. Indeed, a maximum flux of 160 L m^{-2} h^{-1} bar^{-1} was observed with the M-8–SVR membrane (1.5% TiO_2); this was only 70 L m^{-2} h^{-1} bar^{-1} without UV light (as described in Table III). The activated TiO_2 (under UV light) produced OH° and H^{+}; this attracted more water molecules at the surface of the membrane and increased the flux (photoinduced hydrophilicity).

In addition, we found that M-2–SVR (filtration through the microvoids) produced a higher permeate flux (less fouling) than M-2–FVR (filtration through the macrovoids) because of structural differences. Both membranes (M-6–FVR and M-8–FVR) contained microvoid beneath the skin layer (transformed from macrovoids), and their flux values were in close proximity with M-2–SVR (membrane-inherent microvoids). This also showed that a major proportion of fouling was reduced because of the structural transformation from macrovoids to microvoids.

The concept of a structural parameter (S) is usually considered to describe the internal concentration polarization (ICP). ICP occurs inside the porous support layer and can negatively impact the filtration process and reduce the water flux.[39,40] It was observed that NPs help to decrease the S value (a large S value causes a severe ICP), which is controlled by the membrane thickness (l), tortuosity (τ), and porosity [ε; eq. (14)][40]:

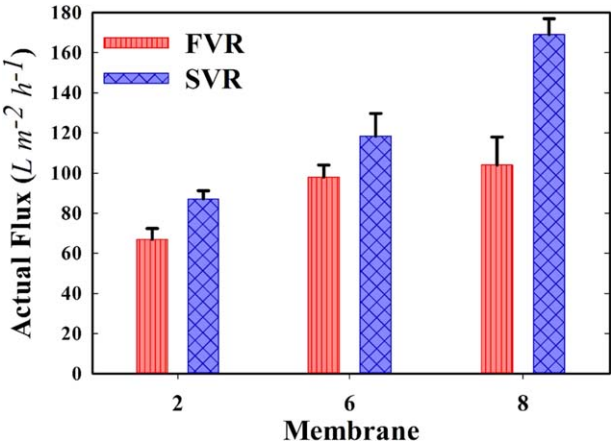

Figure 10. Actual fluxes of membranes (M-2, M-6, and M-8) with different TiO_2 concentrations of 0, 0.5, and 1.5%, respectively, after 90 min of filtration of 2 mg/L HA with UV irradiation. [Color figure can be viewed in the online issue, which is available at wileyonlinelibrary.com.]

Table III. Membrane RF Behavior in Comparison with the Pure Water Flux after 90 min of a UF Experiment with a 2 mg/L HA Solution

Membrane preparation	RF (%)	Actual flux (L m^{-2} h^{-1})	FR (%)	Overall flux decline: 100 − RF (%)	Irreversible flux: 100 − FR (%)	Reversible flux: FR − RF (%)
PP–FVR	22	41	30	78	70	9
PP–SVR	30	51	57	70	43	27
PPT–FVR	30	60	42	70	51	19
PPT–SVR	37	70	75	63	25	38

$$S=\frac{l\tau}{\varepsilon} \tag{14}$$

ε of the membrane can be determined with eq. (15)[41]:

$$\varepsilon=\frac{W_w-W_d}{\rho_{H_2O}A_mL} \tag{15}$$

where W_w is the wet weight of the membrane, W_d is the dry weight of the membrane, A_m is the total membrane area, L is the thickness of the membrane, and $\rho_{H2}O$ is the density of water. τ of the membrane can be determined with the following equation[42]:

$$\tau=\frac{(2-\varepsilon)^2}{\varepsilon} \tag{16}$$

In this study, the addition of NPs reduced the S value from 0.061 mm (M-2) to 0.047 mm (M-6, 0.5% TiO_2) and 0.040 mm (M-8, 1.5% TiO_2). The lowest S value among all of the membranes suggested that the minimum ICP occurred in M-8; this retarded the decreasing flux tendency and further revealed the significant role of the inherent porous structure modified by the incorporation of TiO_2–NPs in the fouling mitigation, especially the effective control of ICP. Hence, the maximum flux was achieved with M-8.

Resistance Analysis

The neat PVDF membrane (M-2) and the membrane containing 1.5% TiO_2 (M-8) were run in the FVR and SVR flow orientations without UV irradiation to assess the preferred flow orientation. Figure 11 shows the normalized fluxes of the neat PVDF (M-2) and 1.5% TiO_2–NP containing membranes (M-8) in the FVR and SVR flow orientations. PP–FVR, PPT–FVR, PP–SVR, and PPT–SVR refer to M-2 (without TiO_2) operated in the FVR mode, M-8 (with 1.5% TiO_2) operated in the FVR mode, M-2 operated in the SVR mode, and M-8 operated in the SVR mode, respectively (PP represents PVDF-PEG membrane, PPT represents PVDF-PEG-TiO_2 membrane). The membranes were vulnerable to fouling in the following order: PP–FVR > PP–SVR > PPT–FVR > PPT–SVR. The neat PVDF membranes were more resistive to fouling in the SVR flow orientation than in the FVR flow orientation. The most resistant membrane to fouling was PPT operated in the SVR flow orientation. These results clearly indicate that the membrane porous structure (Figure 2) played an important role in determining the fouling resistivity; the microvoids at the membrane–solution interface enhanced the fouling resistivity in the PVDF membranes. The PPT–SVR membrane produced 70 L m^{-2} h^{-1} bar^{-1} flux at the end of the 90-min UF experiment compared to 51 L m^{-2} h^{-1} bar^{-1} produced by the PP–SVR membrane. Both membranes were exposed through spongy voids to a pollutant solution. The presence of TiO_2–NPs was responsible for the enhanced membrane flux of the PPT–SVR membrane.

Table III lists data representing the RF behavior of the two membranes after the 90-min UF experiment with 2 mg/L HA solution in two flow orientations. Among these four cases, PP–FVR had the smallest RF of 21%, an actual flux of 41 L m^{-2} h^{-1} bar^{-1}, and an FR of 30%, whereas PPT–SVR had the maximum RF of 37%, an actual flux of 70 L m^{-2} h^{-1} bar^{-1}, and an FR of 75%. The best RF behavior for PPT–SVR was still attributed to the synergistic effect of spongy voids and TiO_2–NP exposure to the HA solution.

With the resistance-in-series model, various resistance results for the M-2 and M-8 membranes with both flow orientations (PP–FVR, PP–SVR, PPT–FVR, and PPT–SVR) were calculated and are summarized in Figure 12. We found that R_m was almost the same with all of the membranes except for PPT–SVR, which had the smallest R_m of 19.1 × 10^{11} m^{-1}. The decrease in R_m of PPT–SVR was due to the exposure of TiO_2 on the membrane surface; this increased the hydrophilicity of the membrane. We also found that the R_{if} values of the membranes in the SVR flow orientation were significantly reduced compared to those

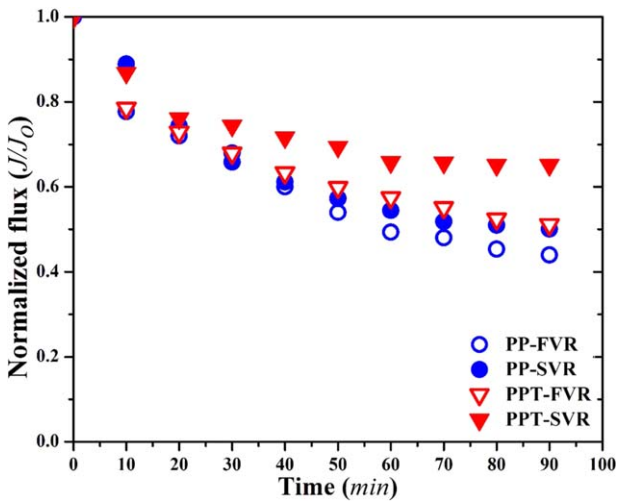

Figure 11. Normalized fluxes of the neat PVDF (M-2) and 1.5% TiO_2–NP containing membranes (M-8) in the FVR and SVR flow orientations. J = flux at any time; Jo = flux at the start of the experiment. [Color figure can be viewed in the online issue, which is available at wileyonlinelibrary.com.]

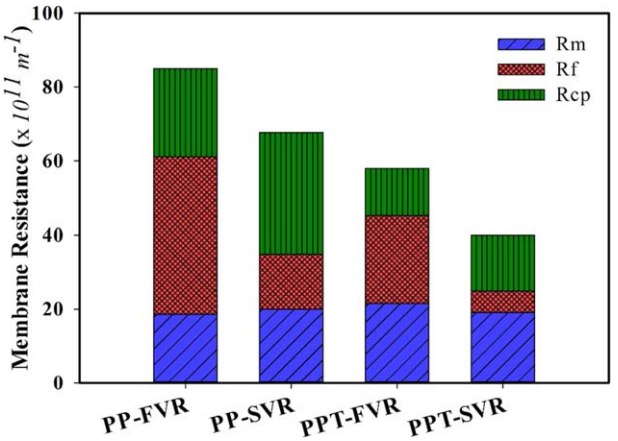

Figure 12. Resistance analysis of the M-2 and M-8 membranes in two flow orientations without UV light. [Color figure can be viewed in the online issue, which is available at wileyonlinelibrary.com.]

in the FVR flow orientation; this was attributed to the microvoid membrane structure facing HA solution. However, we noticed that the R_{cp} value of the membrane was higher in the SVR flow orientation than that in the FVR flow orientation. This was consistent with the fact (Table III) that the reversible flux decline was higher with the SVR flow orientation than with the FVR flow orientation. In addition, Figure 12 indicates an important fact: despite individual resistance considerations, the PPT–SVR membrane had the smallest overall resistance of 40×10^{11} m^{-1} after the 90-min UF experiment.

CONCLUSIONS

In this study, we carefully examined the role of TiO_2–NPs in the inherent membrane structure and their effect on the membrane filtration behavior. We demonstrated that TiO_2–NPs improved the resistance to fouling propensity of the membrane by transforming a macrovoid porous network (beneath the skin layer or top layer) into microvoids. The elemental composition and surface analyses revealed that the TiO_2–NPs were more inclined to be concentrated on the bottom surface of the membrane instead of on the skin surface. Thus, the TiO_2–NPs expressed hydrophilicity mainly when the skin side was down, that is, in the SVR flow orientation. Moreover, the hybrid membrane with a high concentration of TiO_2–NPs in the SVR flow orientation significantly increased the membrane flux and reversible flux decline; more FR and HA rejection was also achieved. This was due to spongy voids at the solid–liquid interface and the greater exposure of hydrophilic additive TiO_2–NPs to the HA solution. In addition, the TiO_2 with UV light induced the photocatalytic degradation of HA in the membrane cell and further increased the membrane flux to 150 L m^{-2} h^{-1} bar^{-1} compared to the value of 70 L m^{-2} h^{-1} bar^{-1} obtained without UV irradiation after 90 min of filtration of the 2 mg/L HA solution. This study is of great significance because it provided some insights into the effect of inherent porous structure resulting from the incorporation of TiO_2–NPs on the membrane fouling control. It will provide meaningful suggestions for practical novel membrane fabrication and engineering applications.

ACKNOWLEDGMENTS

This research was supported by the National Natural Science Foundation of China (contract grant number 21277090), the National Key Science and Technology Project of Water Body Pollution Control and Reclamation (contract grant number 2014ZX07206001), and the National Research Foundation Singapore through its Campus for Research Excellence and Technological Enterprise.

REFERENCES

1. Luo, M.-L.; Tang, W.; Zhao, J.-Q.; Pu, C.-S. *J. Mater. Process. Technol.* **2006**, *172*, 431.
2. Yang, Y.; Zhang, H.; Wang, P.; Zheng, Q.; Li, J. *J. Membr. Sci.* **2007**, *288*, 231.
3. Zhang, C.-H.; Yang, F.-L.; Wang, W.-J.; Chen, B. *Sep. Purif. Technol.* **2008**, *61*, 276.
4. Rajaeian, B.; Heitz, A.; Tade, M. O.; Liu, S. *J. Membr. Sci.* **2015**, *485*, 48.
5. Moghadam, M. T.; Lesage, G.; Mohammadi, T.; Mericq, J.-P.; Mendret, J.; Heran, M.; Faur, C.; Brosillon, S.; Hemmati, M.; Naeimpoor, F. *J. Appl. Polym. Sci.* **2015**, *132*, 1.
6. Damodar, R. A.; You, S.-J.; Chou, H.-H. *J. Hazard. Mater.* **2009**, *172*, 1321.
7. Tahiri Alaoui, O.; Nguyen, Q. T.; Mbareck, C.; Rhlalou, T. *Appl. Catal. A* **2009**, *358*, 13.
8. Leong, S.; Razmjou, A.; Wang, K.; Hapgood, K.; Zhang, X.; Wang, H. *J. Membr. Sci.* **2014**, *472*, 167.
9. Song, H.; Shao, J.; He, Y.; Liu, B.; Zhong, X. *J. Membr. Sci.* **2012**, *405*, 48.
10. Yu, Z.; Liu, X.; Zhao, F.; Liang, X.; Tian, Y. *J. Appl. Polym. Sci.* **2015**, *132*, 41267.
11. Song, H.; Shao, J.; Wang, J.; Zhong, X. *Desalination* **2014**, *344*, 412.
12. Hou, S.-S.; Kuo, P.-L. *Polymer* **2001**, *42*, 2387.
13. Meng, S.; Mansouri, J.; Ye, Y.; Chen, V. *J. Membr. Sci.* **2014**, *450*, 48.
14. Liang, S.; Qi, G.; Xiao, K.; Sun, J.; Giannelis, E. P.; Huang, X.; Elimelech, M. *J. Membr. Sci.* **2014**, *463*, 94.
15. Pekakis, P. A.; Xekoukoulotakis, N. P.; Mantzavinos, D. *Water Res.* **2006**, *40*, 1276.
16. Matilainen, A.; Sillanpää, M. *Chemosphere* **2010**, *80*, 351.
17. Ilyas, H.; Qazi, I. A.; Asgar, W.; Awan, M. A.; Khan, Z.-U.-D. *J. Nanomater.* **2011**, *2011* 1.
18. Im, J.-K.; Son, H.-S.; Kang, Y.-M.; Zoh, K.-D. *Water Environ. Res.* **2012**, *84*, 554.
19. Younas, H.; Qazi, I. A.; Hashmi, I.; Ali Awan, M.; Mahmood, A.; Qayyum, H. A. *Environ. Sci. Pollut. Res.* **2013**, *21*, 740.
20. Le-Clech, P.; Lee, E.-K.; Chen, V. *Water Res.* **2006**, *40*, 323.
21. Ma, N.; Quan, X.; Zhang, Y.; Chen, S.; Zhao, H. *J. Membr. Sci.* **2009**, *335*, 58.
22. Yeow, M. L.; Liu, Y. T.; Li, K. *J. Appl. Polym. Sci.* **2004**, *92*, 1782.

23. Bohonak, D.; Zydney, A. *J. Membr. Sci.* **2005**, *254*, 71.
24. Oh, S. J.; Kim, N.; Lee, Y. T. *J. Membr. Sci.* **2009**, 345, *13*.
25. Shao, J.; Hou, J.; Song, H. *Water Res.* **2011**, *45*, 473.
26. Vergili, I. *J. Environ. Manage.* **2013**, *127*, 177.
27. Lu, X.; Arias Chavez, L. H.; Romero-Vargas Castrillón, S.; Ma, J.; Elimelech, M. *Environ. Sci. Technol.* **2015**, *49*, 1436.
28. Li, W.; Ni, C.; Lin, H.; Huang, C. P.; Shah, S. I. *J. Appl. Phys.* **2004**, *96*, 6663.
29. Cao, J.; Wang, L.; Shang, Y.; Fang, M.; Deng, L.; Gao, J.; Li, J.; Chen, H.; He, X. *Electrochim. Acta* **2013**, *111*, 674.
30. Ismail, A. F.; Hassan, A. R. *J. Membr. Sci.* **2006**, *270*, 57.
31. Mostafa, K. M. G.; Liu, C.-Q.; Sakugawa, H.; Vione, D.; Minakata, D; Wu, F. Photobiogeochemistry of Organic Matter: Principles and Practices in Water Environment; Springer: Berlin, **2013**.
32. Athanasekou, C. P.; Morales-Torres, S.; Likodimos, V.; Romanos, G. E.; Pastrana-Martinez, L. M.; Falaras, P.; Dionysiou, D. D.; Faria, J. L.; Figueiredo, J. L.; Silva, A. M. T. *Appl. Catal. B* **2014**, *158*, 361.
33. Antonopoulou, M.; Evgenidou, E.; Lambropoulou, D.; Konstantinou, I. *Water Res.* **2014**, *53*, 215.
34. Liang, S.; Kang, Y.; Tiraferri, A.; Giannelis, E. P.; Huang, X.; Elimelech, M. *ACS Appl. Mater. Interfaces* **2013**, *5*, 6694.
35. Devi, S.; Ray, P.; Singh, K.; Singh, P. S. *Desalination* **2014**, *346*, 9.
36. Chandran, P.; Netha, S.; Sudheer Khan, S. *J. Photochem. Photobiol. B* **2014**, *138*, 155.
37. Khan, S.; Kim, J.; Sotto, A.; Van der Bruggen, B. *J. Ind. Eng. Chem.* **2015**, *21*, 779.
38. Pansamut, G.; Charinpanitkul, T.; Biswas, P.; Suriyawong, A. *Eng. J.* **2013**, *17*, 25.
39. Wei, J.; Qiu, C.; Tang, C. Y.; Wang, R.; Fane, A. G. *J. Membr. Sci.* **2011**, *372*, 292.
40. Yin, J.; Deng, B. *J. Membr. Sci.* **2015**, *479*, 256.
41. Emadzadeh, D.; Lau, W. J.; Matsuura, T.; Ismail, A. F.; Rahbari-Sisakht, M. *J. Membr. Sci.* **2014**, *449*, 74.
42. Srisurichan, S.; Jiraratananon, R.; Fane, A. *J. Membr. Sci.* **2006**, *277*, 186.